Surface energy of hydroxyapatite and *β*-tricalcium phosphate ceramics driving serum protein adsorption and osteoblast adhesion

E. A. dos Santos · M. Farina · G. A. Soares · K. Anselme

Abstract The main objective of this work was to evaluate the specific role of calcium phosphates surface energy on serum protein adsorption and human osteoblast adhesion, by isolating chemical effects from those caused by topography. Highly dense phosphate ceramics (single-phase hydroxyapatite HA and *β*-tricalcium phosphates *β*-TCP) presenting two distinct nano roughnesses were produced. Some samples were gold-sputter coated in order to conveniently mask the surface chemical effects (without modification of the original roughness) and to study the isolated effect of surface topography on cellular behavior. The results indicated that the nano topography of calcium phosphates strongly affected the protein adsorption process, being more important than surface chemistry. The seeding efficacy of osteoblasts was not affected nor by the topography neither by the calcium phosphate chemistries but the *β*-TCP chemistry negatively influenced cell spreading. We observed that surface hydrophobicity is another way to change protein adsorption on surfaces. The decrease of the polar component of surface energy on gold-coated samples leaded to a decreased albumin and fibronectin adsorption but to an increased cell adhesion.

E. A. dos Santos · G. A. Soares
Dep. de Eng. Metal. e de Materiais, COPPE/UFRJ, CP 68505,
Rio de Janeiro 21941-972, Brazil

E. A. dos Santos · K. Anselme (✉)
Institut de Chimie des Surfaces et Interfaces/UPR CNRS 9069,
15 rue Jean Starcky, BP 2488, 68057 Mulhouse, France
e-mail: karine.anselme@uha.fr

M. Farina
Lab. de Biomineralização, ICB/UFRJ,
Rio de Janeiro 21941-590, Brazil

Overall, this work contributes to better understand the role of topography and surface chemistry of calcium phosphates in serum protein adsorption and osteoblast adhesion.

1 Introduction

Surface energy directly influences two important phenomena for an efficient cell/biomaterial interaction: proteins adsorption [1] and cell attachment [2]. Interfaces exhibit generally chemical bonds of surface atoms asymmetrically directed toward the interior of the material, attracting the surface atoms inward and causing surface tension. The energy of exposed surface groups decreases by adsorbing or reacting with ambient molecules. As a result, the first stage after implantation of a biomaterial into the body involves protein adsorption. After immersion in biological fluids, all implant materials are coated by a protein layer, and the presence of this pre-adsorbed protein layer is essential in mediating cell response to the material.

Calcium phosphate ceramics have been widely used for clinical applications in bone grafting and orthopedics, and they display a very high adsorption capacity for serum proteins compared with other implant materials [3]. Particularly, previous studies have shown that HA adsorbs more fibronectin and vitronectin than titanium and steel surfaces [3, 4]. These proteins are typically found in serum, and they contain well-known ligands, like the Arg–Gly–Asp (RGD) amino acid sequence, which is selectively recognized by cellular receptors (i.e. integrins), mediating cell adhesion to the substrate [5, 6]. When an integrin-mediated adhesion occurs, the transmembrane receptors begin to cluster and initiate signalling cascades that

ultimately drive events such as cell spreading, migration, proliferation, and differentiation.

The protein adsorption process is a function of substrate composition, given that proteins can dissociate at a suitable pH, resulting in ionic species (R-COO$^-$ and R-NH$_3^+$). Thus, proteins can interact not only with positively or negatively charged surfaces (electrostatic interactions) but also with neutral surfaces by means of hydrophobic interactions. For calcium phosphate ceramics, protein adsorption has an electrostatic nature, once Ca^{2+} and PO$_4^{3-}$ ions are believed to provide the major driving force in this process [4, 7]. Additionally, Luo et al. [8] suggest that the affinity of the Ca^{2+} site in HA for negative charge (COO$^-$) of proteins is larger than that of the PO$_4^{3-}$ sites in HA for positive charge (NH$_3^+$) of proteins.

On the other hand, surface topography can also significantly influence protein adsorption [9–11]. Then, one of the main problems found in several works that study protein adsorption and cell adhesion on materials surface is the difficulty in correctly discriminating topographical effects from those produced by the proper surface chemistry. Generally, the authors point out a possible contribution of topography, but the particular role played by each variable is not well defined. Accordingly, the main objective of this work was to evaluate the specific role of calcium phosphates surface energy on serum protein adsorption and cell adhesion, by conveniently isolating chemical effects from those caused by topography.

2 Materials and methods

2.1 Production of dense surfaces (HA and β-TCP)

Stoichiometric hydroxyapatite (HA) powder, obtained by the wet precipitation method [12] in the Brazilian Center for Physical Research (CBPF), was used to produce HA samples. Tricalcium phosphate (TCP, Merck) was used to produce β-TCP samples. Tablets with 7.6 mm diameter and 1.0 mm height were made by uniaxial pressing of HA and TCP powders under a load of 216 MPa. After pressing, the obtained tablets were calcined at 1,150 °C for 4 h in order to produce a dense surface structure. No grinding of samples was done before in vitro experiment in order to keep intact the surface nano topography inherently formed after calcination. The relative density of the tablets after calcination was calculated by the geometrical approach, comparing theoretical and experimental (mass/geometrical volume) densities. Theoretical densities used for HA and β-TCP were 3.16 g/cm^3 and 3.07 g/cm^3, respectively [13].

2.2 Surface coating

The half of the original samples was gold-sputter coated in order to mask the surface chemical effects and to study the effect of topography on cellular behavior. The coating was performed using an Edwards (Scancoat Six) sputter coater for scanning electron microscopy preparation. The distance between the gold source and samples was 3 cm. The coating was done under a current of 20 mA during 2 min, in order to obtain an about 15 nm film thickness.

2.3 Surface characterization

2.3.1 Morphological aspects

After calcination, the samples were examined by scanning electron microscopy (SEM) in a JEOL JSM 6460LV microscope to investigate whether pores or other not desired surface patterns like grooves or cracks were present. Surface microporosity was measured on digital images acquired by SEM using backscattered electrons. The digital images were processed by using Global Lab Image$^{\circledR}$ software. Atomic force microscopy (AFM) was used to characterize surface roughness (R$_a$) of ceramics. Two square images (400 μm^2) were taken from different regions for six samples (each condition) using the tapping mode in an AFM Multimode Nanoscope IV. The gold-coated surfaces were equally analyzed by AFM to check possible topography modifications. Gold and ceramic can be easily discriminated by SEM using backscattered electrons. Thus, the gold coating homogeneity on surfaces was qualitatively evaluated by this method. The gold thickness on samples was estimated from cross sections perpendicular to the surfaces using TEM after resin embedding and ceramic dissolution. Moreover, the coating stability in medium culture was similarly monitored along time.

2.3.2 Sample composition

The chemical composition of the samples after calcination was investigated using XRD. All samples were submitted to analysis after grinding. XRD patterns were performed from $2\theta = 10°$ to $100°$ (step size of $0.05°$ and scanning speed of $1°$/min) in a RIGAKU MINIFLEX powder diffractometer. The obtained unit-cell parameters of HA and β-TCP (a, b and c) were refined using Celref software (JCPDS, cards No. 9-432 and 9-169 for HA and β-TCP, respectively).

2.3.3 Surface energy

The contact angle θ was calculated using three liquids with known dispersive γ_L^D, polar γ_L^P and total surface energy γ_L ($\gamma_L = \gamma_L^D + \gamma_L^P$) values: water ($\gamma_L = 72.8$; $\gamma_L^D = 21.8$ e $\gamma_L^P = 51.0$ mJ m^{-2}), glycerol ($\gamma_L = 64.0$; $\gamma_L^D = 34.0$ e $\gamma_L^P = 30.0$ mJ m^{-2}) and di-iodomethane ($\gamma_L = 50.8$; $\gamma_L^D = 50.8$ e $\gamma_L^P = 0.0$ mJ m^{-2}) [14, 15]. The measurements were performed in a goniometer (Krüss, G2) after sterilization (180 °C/2 h under air) of the original samples. Two drops around 20 μL were deposited on different regions of each sample for a total of six samples (each condition). The gold-coated surfaces were also analyzed under the same conditions.

The dispersive and polar components of the samples surface energy were estimated using the geometrical mean approach according to Owens et al. [16] by the equation

$$(1 + \cos\theta)\gamma_L = 2[(\gamma S^D \gamma L^D)^{1/2} + (\gamma S^P \gamma L^P)^{1/2}],$$

where the superscript D labels the dispersive component and P the polar component of the surface tension. This theory, also referred as the harmonic mean method, considers that two distinct components constitute surface energy: dispersive and polar contributions. The dispersive component γ_S^D refers to van der Waals and other non-site specific interactions between solid surface and an applied liquid. Hydrogen bonding, dipole-dipole, dipole-induced dipole and other site-specific interactions are related to the polar component γ_S^P. Then, adhesion processes on solid surfaces are strongly affected by these two components being crucial its characterization.

2.4 Specific serum proteins adsorption

The adsorption of specific serum proteins, such as albumin (more abundant protein in serum) and fibronectin was investigated by enzyme linked immunosorbent assay (ELISA). The samples (original and gold-coated) were previously immersed for 2 and 24 h in McCoy's 5A culture medium supplemented with 10% FBS and antibiotics at 37 °C under a humidified atmosphere of 95% air and 5% CO_2. After incubation, the tablets were washed in PBS and transferred to clean 24-well culture plates. A 3% skimmed milk solution in PBS containing 0.3% Tween was added to the samples for 1 h at 37 °C to block non-specific adsorptions of detecting antibody on the surfaces. After blocking, the samples were washed in PBS, and the primary antibody (mouse IgG anti BSA or anti FN) was added and incubated at 37 °C for 1 h. Any excess antibody was then discarded by aspiration from the wells, which were washed with PBS three times. The secondary antibody (Goat anti mouse IgG coupled to alkaline phosphatase) was added to react with primary antibody for 1 h at 37 °C. Following rinsing with PBS, the samples were filled with 200 μL of alkaline phosphatase (ALP) substrate kit (Bio-Rad) and incubated at 37 °C for 30 min. The reaction was stopped by the addition of 200 μL of 0.4 mol/L NaOH. The reaction solution was transferred to a 96-well plate and absorption was measured at 405 nm using a microplate reader (ELX800UV, Bio-Tec Instruments, INC). The assays were performed in triplicate.

2.5 Osteoblast culture on the original and gold-coated surfaces

Human osteoblastic cells (SaOs2) at 6th passage were cultured in 75 cm^2 flasks containing McCoy's 5A Medium Modified (Sigma) supplemented with 10% fetal bovine serum (FBS) and antibiotics (100 U/mL penicillin and 100 μg/mL streptomycin) in an incubator at 37 °C under a humidified atmosphere of 95% air and 5% CO_2. After confluence, the cells were trypsinized, resuspended in complete medium and counted in a Malassez hemocytometer. The ceramic samples were sterilized by heating under air at 180 °C for 2 h. The sterilization by autoclaving was replaced because of the possible induction of surface phase transformation and β-TCP dissolution. The samples were placed into a culture plate coated with agar gel (2% in water) to avoid cell growth on the bottom of the well and immersed in 500 μL of McCoy's 5A culture medium supplemented with 10% FBS and antibiotics. Then, 500 μL of a cell suspension containing 4.0×10^4 cells in the 7th passage were seeded on each tablet. Initial cell adhesion was monitored after 4 and 24 h in culture. Tissue culture plastic coverslips (Thermanox®, NUNC™, USA) were used as controls. A total of three independent assays were carried out for each experiment, with each assay performed in triplicate.

2.6 Seeding efficacy

Seeding efficacy is based on the ratio between the number of adhering cells (after 4 h in culture) and the total number of adhered cells on the control. Thus, this value indicates the initial affinity of cells/substrate. Quantification of viable cells on the samples was performed by an MTT assay. At each time point, the samples were slightly rinsed with PBS solution to remove non-adhered cells. 400 μL of 5 mg/mL MTT [3-(4,5-dimethylthiazol-2-yl)-2,5-diphenyl tetrazolium bromide] (Sigma) were added to the remaining cells and incubated for 4 h at 37 °C under a humidified atmosphere of 95% air and 5% CO_2. Afterwards, the MTT was removed and the cells were

immersed in 300 μL of acidic isopropanol under shaking to dissolve intracellular formazan crystals produced by viable cells. Absorbance was determined at 570 nm using an ELISA reader. Cell number was obtained using a linear correlation between absorbance and SaOs2 cell concentration (from 0.5×10^4 up to 2×10^4 cells/mL). The results from three individual experiments (in triplicate, $n = 9$) were averaged.

2.7 Cell spreading

Cell spreading on both original and gold-coated surfaces after 24 h in culture was quantified using fluorescence microscopy. All measurements were accomplished on digital images obtained from an epifluorescent microscopy system and processed by Global Lab Image® software. The evaluation was based on the ratio between the area occupied by one isolated cell and the total area of the image. At least 40 cells, localized in different regions of the same surface, were used for this quantification, and a total of two independent assays was carried out.

2.8 Statistical analysis

The statistical significance of the obtained data was assessed using two-way ANOVA variance analysis and the Tukey Test. Differences at $P \geq 0.05$ were considered statistically not significant.

3 Results

3.1 Sample characterization

3.1.1 Surface morphology

After calcination at 1,150 °C, shrinkages of approximately $18.9 \pm 1.0\%$ in the diameter of the HA samples, and of $17.9 \pm 0.6\%$ for the β-TCP were observed. The relative density of HA ($95 \pm 2\%$) was higher than that calculated on β-TCP ($79 \pm 2\%$). Despite this values, dense surface structures were observed for HA and β-TCP samples (Fig. 1). In fact, the relative surface microporosity measured on each sample had low values, being of 0.01% for HA and 0.67% for β-TCP. Surface patterns like grooves or cracks were not seen though important differences between the two surface topographies were noticed. The grains on the β-TCP surface were bigger than those on the HA one. As expected, the average surface roughness (R_a) value was higher on the β-TCP surface (142 ± 24 nm) than on HA (32 ± 6 nm).

After coating with gold, there was no significant difference between the surface roughness (R_a) of the HA[Au] (33 ± 3 nm) and of the HA original surface ($P > 0.05$). Similarly, there was no significant difference between the

Fig. 1 SEM micrographs of the HA (**a**, **c**) and β-TCP (**b**, **d**) surfaces after calcination at 1,150 °C for 4 h
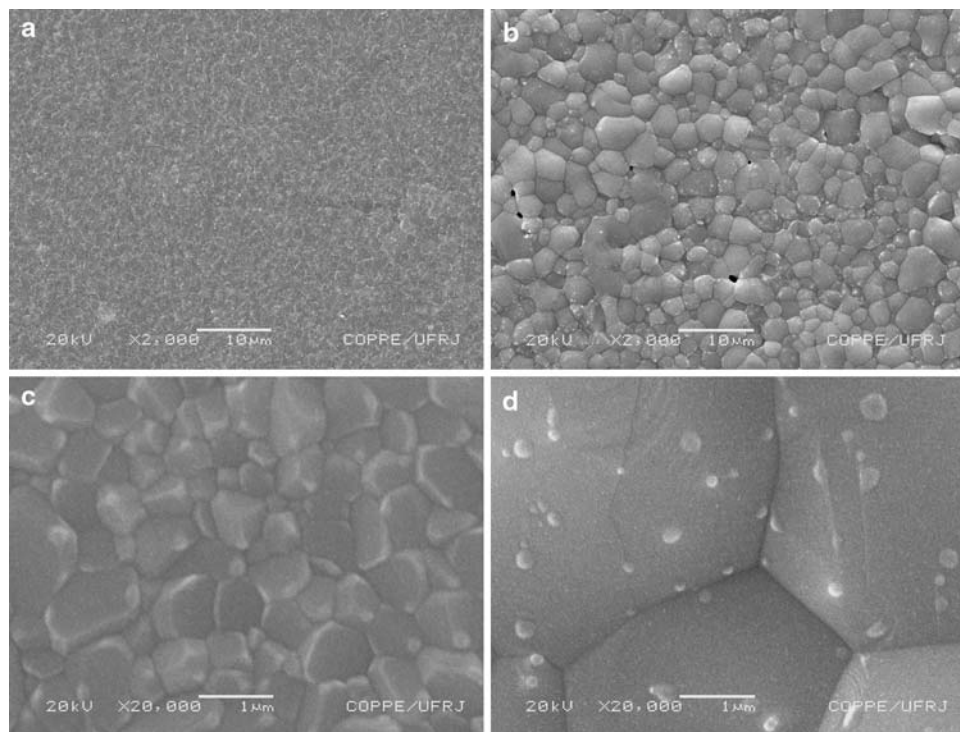
β-TCP[Au] roughness (144 ± 15 nm) relatively to the β-TCP original surface, suggesting that original roughness was preserved at this nano scale. Besides, the images acquired by SEM (backscattering electrons) in different regions of gold coating samples did not present defects or discontinuity along surfaces, indicating a homogeneous distribution. The average gold thickness was estimated around 20 nm using TEM, and it was stable along culture as no variations were verified (data not shown).

3.1.2 Chemical composition

XRD patterns of the HA and β-TCP samples after calcination confirmed the presence of pure ceramics (Fig. 2). The three maximum diffraction peaks corresponding to the planes (2 1 1), (1 1 2) and (3 0 0) for HA were seen at 31.8°, 32.2° and 32.9° respectively. No phase transformation was observed, as the diffraction intensities at $2\theta = 30.7°$ (0 3 4) and 31.0° (0 2 10) corresponding to the allotropic forms α-TCP and β-TCP respectively, was not significant. The three maximum diffraction peaks corresponding to the planes (0 2 10), (2 2 0) and (2 1 4) of β-TCP were observed at 31.0°, 34.4° and 27.8°. The allotropic form α-TCP was not found at a relevant concentration as shown by the spectra, since the diffraction intensity at $2\theta = 30.7°$ (0 3 4) was not significant.

3.1.3 Surface energy

The total surface energy γ_S was equivalent on the HA and β-TCP surfaces (Fig. 3). The polar component γ_S^P was
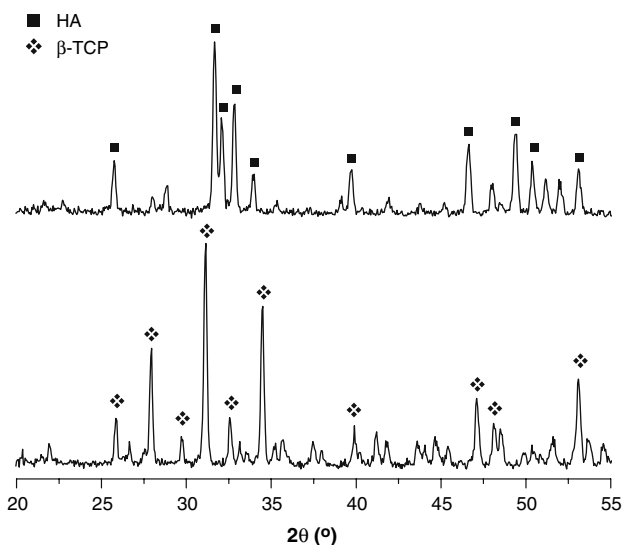

Fig. 2 XRD spectra of the HA and β-TCP samples after calcination at 1,150 °C for 4 h. The ten most intense diffraction peaks for each phosphate are shown on the patterns
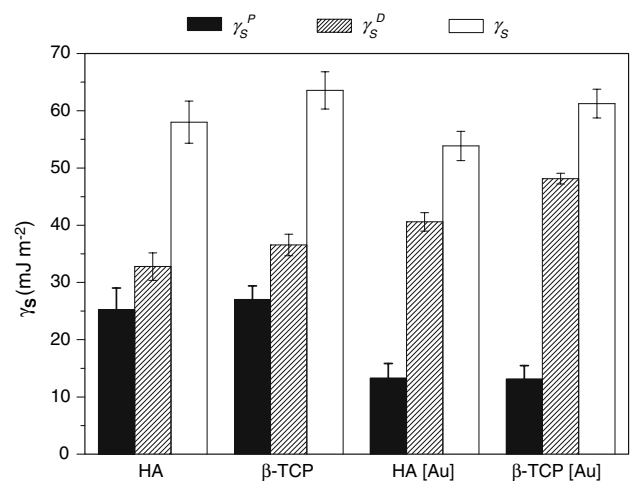

Fig. 3 Surface wettability of the original and gold-coated surfaces and its polar γ_S^P, dispersive γ_S^D and the total surface tensions γ_S

smaller than the dispersive one γ_S^D on all surfaces ($P < 0.05$). Besides, gold coating induced a significant decrease of this component whereas it induced an increase of the dispersive component when compared with the original surfaces. However, coating did not modify total surface energy (sum of the polar and dispersive component) in relation to original surfaces ($P > 0.05$).

3.1.4 Protein adsorption

The quantity of albumin adsorbed at 2 h was similar ($P > 0.05$) on the HA and β-TCP surfaces (Fig. 4). No variation was observed along time. However, on the gold coated surfaces, a higher adsorption was observed on HA relatively to β-TCP. Similarly to the original surfaces, no significant variation was verified along time on each surface.
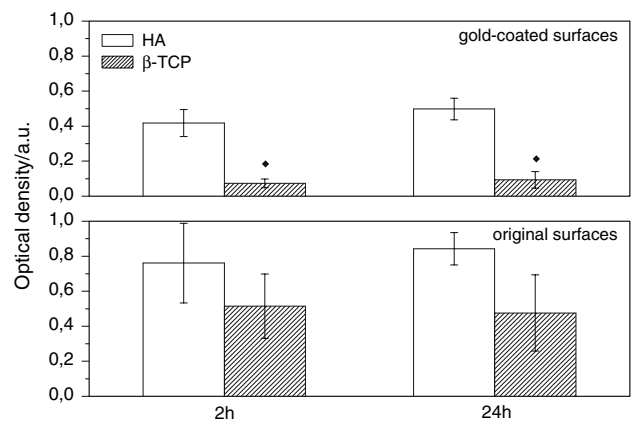

Fig. 4 Adsorption of albumin on the HA and β-TCP (original and gold-coated surfaces) along time in culture medium supplemented with 10% FBS at 37 °C. Significant difference ($P < 0.05$) between HA and β-TCP ($\blacklozenge$)
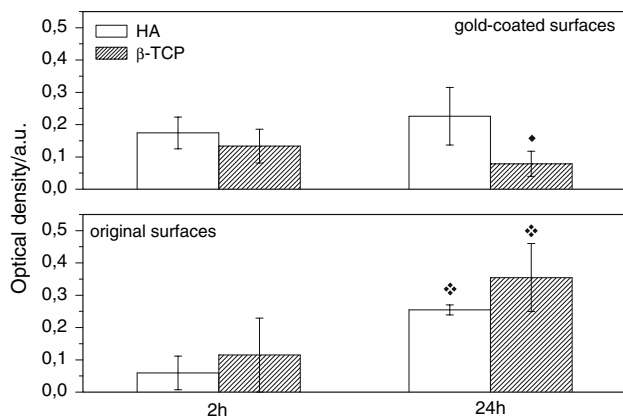
Fig. 5 Adsorption of fibronectin on the HA and β-TCP (original and gold-coated surfaces) along time in culture medium supplemented with 10% FBS at 37 °C. Significant difference ($P < 0.05$) between HA and β-TCP (♦). Significant difference ($P < 0.05$) between 2 h and 24 h (❖)

In general, a higher protein quantity was observed on original surfaces when compared to the gold-coated ones.

The fibronectin was found on the original surfaces in similar quantities comparing HA and β-TCP surfaces (Fig. 5). However, fibronectin adsorption significantly increased along time on the two surfaces. On the gold coated surfaces, the quantity of protein on each surface was the same along time but after 24 h a higher adsorption was measured on the HA relatively to the β-TCP.

3.2 Cell adhesion

3.2.1 Seeding efficacy

After 4 h in culture, the same number of cells was found on the uncoated surfaces (Fig. 6). After gold coating, despite the amount of adhered cells significantly increased
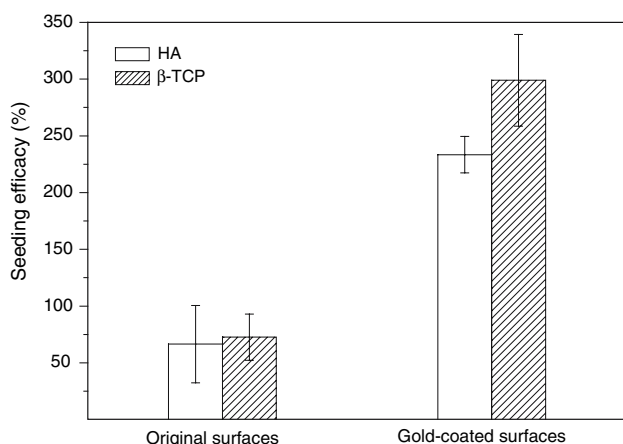
relatively to the original surfaces ($P < 0.05$), no difference was observed between the two surfaces ($P > 0.05$). When compared with the control, the adhesion on the coated surfaces was approximately three times higher than that on the original surfaces.

3.2.2 Cell spreading

After 1 day in culture, the average area occupied by one cell on HA was significantly higher than that measured on β-TCP surfaces (Fig. 7). A similar spreading was observed on the gold-coated surfaces. Comparing only the β-TCP surfaces, the original surface displayed a lower cell spreading than the gold-coated one. No difference of spreading was observed after coating of the HA substrates.

4 Discussion

Biological responses to an implant are determined not only by surface topography but also by chemistry and, consequently, by the surface energy of the material [17–19]. The relative effect of either topography or chemistry is generally difficult to discriminate. Thus, to evaluate both HA and β-TCP chemical effects on serum protein adsorption and osteoblast adhesion, we tried to control the topographical aspects of the studied surfaces. In this direction, surface densification was one of the primary objectives of this work. Despite the low surface microporosity, the HA and β-TCP surfaces presented different nano roughnesses due to the inherent grain growth during thermal treatment (Fig. 1).

Biphasic compounds (HA/TCP) have lower shrinkages than pure HA [20–22]. During calcination, the bonding phenomenon between two particles will take place in order to decrease the total surface area by means of a diffusion
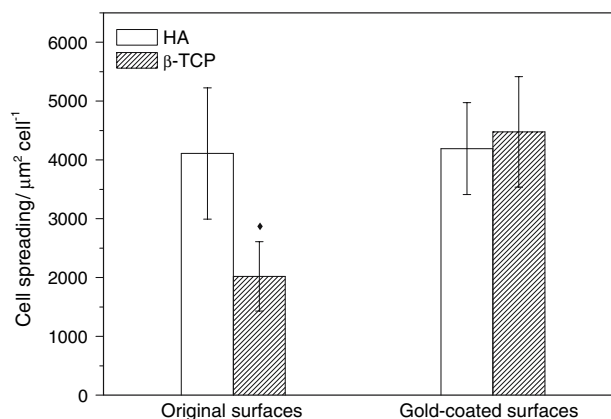

Fig. 6 Ratio between the number of adhering cells on the samples and the number of cells adhering on the control after 4 h in culture

Fig. 7 Cell spreading on the original and gold-coated surfaces after 1 day in culture. Significant difference ($P < 0.05$) between HA and β-TCP (♦)

process [23]. The specific surface area decrease in β-TCP samples, resulting from its low coalescence temperature (below 700 °C), would have promoted a remarkable grain growth when compared with the HA ceramics. This hypothesis could explain the surface morphologies observed on our β-TCP surfaces.

In order to mask the surface chemical effects and to study the relative effect of topography on cellular behaviour, we proceeded to the coating of the samples by gold-sputtering. Obviously, gold coating is inappropriate in terms of in vivo implants but, in this work, it was used only as a tool for masking the original chemistry of the samples and to relate serum protein adsorption and cell adhesion to surface topography. Thus, the differences in protein adsorption and cell adhesion on the gold-coated HA and β-TCP surfaces can be related to the surface topography since the two surfaces present the same chemical composition (gold). As expected, gold coating did not modify the initial surface roughness (R_a). However, surface wettability was significantly affected (Fig. 3). Although there were no changes in the total surface tension γ_S after gold coating, the polar component γ_S^P significantly decreased whereas the dispersive component γ_S^D increased, indicating that the hydrophobicity of the surfaces was increased. Wettability degree is a direct function of surface chemical composition, but it can be also affected by topography. Chemical heterogeneities and surface roughness are among the main variables that influence the hysteresis phenomenon in contact angle measurements [24]. In our case, as the gold-coated surfaces had the same chemical composition, it appears that the differences in topographies exhibited by the HA[Au] and β-TCP[Au] were not sufficient to influence surface wettability.

4.1 Topographical relative effects on protein adsorption

It is known that the spatial distribution of adsorption sites on surface can improve or impair adsorption process [8]. Thus, the surface topography is a concrete way for creating differences in geometrical disposition of adsorption sites. To study only the influence of HA and β-TCP topographies on protein adsorption we firstly focused our attention on the gold-coated surfaces. The albumin adsorption on the HA[Au] was higher than that observed on the β-TCP[Au] along time (Fig. 4). Besides, the quantity of fibronectin was also higher on the HA[Au] than on β-TCP[Au] after 24 h (Fig. 5). Overall, it seems that the differences of topography displayed by HA[Au] and β-TCP[Au] surfaces have a strong effect on protein adsorption.

Recently, Cai et al. [9] showed that a nanometer scale roughness on titanium surfaces (2–20 nm) had little effect on the structure and amount of adsorbed albumin and fibringen. On the other hand, Dufrene et al. [11] showed that the adsorption of larger molecules like collagen can be affected by different roughness degrees of polymer surfaces. It was observed not only differences on the amount of adsorbed proteins but also on their structure. Some authors have speculated that when the roughness scale increases from nanometers to micrometers, exceeding the protein size, topography may appear smooth to the protein, inducing minimal effects on adsorption process [25, 26]. This can explain the higher albumin adsorption on the HA[Au] surface, exhibiting surface roughness comparable to the albumin dimensions (~ 10 nm). Conversely, as the β-TCP[Au] nano roughness is much larger than that of albumin, it did not produce significant effects on the albumin adsorption along time.

The results obtained for fibronectin suggest that the surface roughness did not affect adsorption at 2 h. However, the HA[Au] roughness was more adequate for fibronectin adsorption than β-TCP[Au] one after 24 h. This fact can be explained by the fact that protein adsorption from serum is a complex dynamic process. Proteins can be initially adsorbed but, subsequently, replaced by other proteins in a competition for sites or thermodynamic stabilization [27]. In the present work, this phenomenon seems basically be driven by topography, independently of original surface composition.

For the HA[Au] samples, the ratio between grain boundary areas and the total area of surface is probably larger than that observed on the β-TCP[Au]. Grain boundaries are generally associated to a high surface energy. Besides, the geometry exhibited by these regions could significantly increase the number of interactions protein/gold. These facts point to an alternative explanation for the higher adsorption of protein generally observed on the HA[Au] surfaces.

4.2 Chemical relative effects on protein adsorption

The studied surfaces presented essentially three kinds of chemistry: hydroxyapatite (HA), β-tricalcium phosphates (β-TCP) and gold (coated surfaces). Thus, to evaluate the chemical effects on protein adsorption it was necessary to separate the effects caused by the original phosphate chemistry (HA/β-TCP) of those induced by gold coating (HA/HA[Au] and β-TCP/β-TCP[Au]).

4.2.1 Comparison of uncoated/coated surfaces

By comparing the protein adsorption behavior on original and gold-coated surfaces, a strong chemical effect was

noticed. The amount of albumin measured on the original surfaces was slightly higher than that on the gold-coated surfaces (Fig. 4). This phenomenon could be explained by surface energy changes. The decrease of the polar component γ_S^P and, at the same time, the increase of the dispersive component γ_S^D (Fig. 3) induced by gold coating considerably reduced adsorption compared to the original surfaces. It is known that hydrophobic interactions and those of electrostatic character are the main forces that bind proteins to surfaces. Particularly in the case of calcium phosphates, electrostatic interactions are most probable since negatively or positively charged proteins can easily interact with positive or negative groups of these phosphates [4]. According to Luo et al. [8], the generally negatively charged surface of HA is greatly suppressed by the adsorption of Ca^{2+} ions proceeding from the original HA dissolution. The resultant surface positive charges can easily interact with the protein COO^- groups. Thus the high dispersive component of surface energy on gold-coated surfaces does not favor protein adsorption, as compared to original surfaces.

4.2.2 Comparison of original HA/TCP surfaces

No significant differences were found on the surface energy and wettability values measured on original HA and β-TCP surfaces. At the same time, a similar quantity of adsorbed proteins was found on these surfaces along time in the culture medium. Therefore, the chemical differences exhibited by HA and β-TCP surfaces were not capable of influencing surface energy and, consequently, protein adsorption.

4.3 Cell adhesion

If we compare original HA and β-TCP surfaces, a good relation can be observed between the measured surface free energies and the seeding efficacy (Fig. 3, and Fig. 6). No variations were observed between surface energies on the coated surfaces and, consequently, no variations were observed between seeding efficacies demonstrating that the surface topography has few influence on initial cell adhesion. However, comparing coated and uncoated surfaces, the major hydrophobic character of the gold-coated surfaces leaded to a higher osteoblast adhesion. This fact suggests that the initial cell adhesion (4 h after seeding) was an event basically driven by the surface wettability. Hallab et al. [28] confirmed that, under certain conditions, surface energy can be more important than surface roughness for cell adhesion. In this experiment we observed a higher cell attachment after 4 h on gold-coated hydrophobic surfaces. A lot of in vitro experiments have

used model surfaces like SAMs, polymer or wettability gradient surfaces for studying the influence of surface energy on protein adsorption and cell adhesion. On wettability gradient surfaces coated with fibronectin, Kennedy et al. demonstrated that the adhesion, spreading and proliferation of murine MC3T3-E1 osteoblastic cells increased with contact angle demonstrating that these cells, by the intermediate of fibronectin, adhered and grew more on hydrophobic part of the gradient [2]. However, this study is in contradiction with the results of a lot of other studies which demonstrated that cell growth decreased on surface with lower wettability [29–31] or that moderately hydrophilic surfaces (20–40 degrees water contact angle) promoted the highest levels of cell attachment [32–36]. Moreover, Keselowski et al. demonstrated on SAMs surfaces (OH, COOH, CH_3, NH_2) presenting different wettabilities that the adsorption of fibronectin on the more hydrophobic surfaces (CH_3 and NH_2) destroyed $\alpha5\beta1$ integrin binding and consequently cell adhesion [30]. The same was observed by Kowalczynska et al. [37, 38].

In all these previous examples, the authors have only considered the contact angle measurement and have correlated this angle with the protein adsorption and/or cellular behaviour. Few authors have attempted to quantify the different components of surface energy and to correlate them to the cell response. It is generally considered that enhancing the polar component of the surface energy rather promotes the initial cell attachment [39, 40]. On the contrary, Ponsonnet et al. [41] have demonstrated on titanium that a low polar component γ_S^P was the major parameter for good fibroblast proliferation, the dispersive component being exactly the same for all their samples. Santiago et al. have observed the same behavior on mice osteoblastic cells cultured on titanium submitted to three different chemical treatments [42].

Among these studies only one concerns the characterization of the polar and dispersive components of surface energy of ceramic materials and the study of their influence on cell adhesion [39]. In this work, Redey et al. demonstrated that the higher polar component of the surface of dense HA ceramics could be related to the higher osteoblastic cell attachment on these ceramics compared to carbonated apatite since the dispersive component on the two materials was comparable [39]. However, they did not study the contribution of protein adsorption and a possible topographical effect on osteoblast adhesion.

A remarkable decrease of cell spreading was observed on β-TCP surface comparatively to the others surfaces, suggesting a strong chemical effect on this process (Fig. 7). Several works have demonstrated that cell spreading is highly dependent on the nature and conformation of adsorbed proteins, and these features of protein adsorption are regulated by the affinity of proteins for the substrata.

Substantial evidences show that specific serum proteins such as fibronectin and vitronectin have an important role in osteoblast spreading. Integrin-binding domains present in these proteins, such as RGD (tripeptide, arginine-glycine-aspartic acid), are recognized by cells and actively promote cellular spreading [43]. In our case, no direct relation was observed between the spreading process and the quantity of fibronectin on each surface after 1 day.

Recently, Sawyer et al. have observed that mesenchymal stem cells were not able to spread on HA coating with RGD, suggesting that the RGD domain alone is not sufficient to promote full cell spreading [6]. Besides, they verified that cell spreading was attenuated by mechanisms other than a lack of FN availability in presence of serum, what suggest that cell spreading was particularly influenced by the presence of other adsorbed serum factors. Cooperative interactions between adsorbed proteins from serum were important for regulating cell spreading. Actually, the biological activity of short peptides coated on substrates is lower than that of the complete protein, as RGD binding integrins need the presence of other peptides to adhere to a substrate. In several cases, the adsorption process can induce conformational changes on proteins masking some peptide sequences and, consequently, affecting cell behavior. Therefore, the adsorption of other proteins or molecules could be also involved in the cell response to the tested ceramics.

5 Conclusion

Overall, a significant contribution of our present work is the precise characterization of the polar and dispersive components of surface energy of two ceramics and their correlation with the protein adsorption and human osteoblast adhesion capacity. The results indicated that the nano topography exhibited by the calcium phosphates studied in this work strongly affected the protein adsorption process, being more important than calcium phosphate chemistry. The nano topography exhibited by HA samples was more favorable to albumin and fibronectin adsorption than the one of β-TCP. The seeding efficacy of osteoblasts was not affected nor by the topography neither by the calcium phosphate chemistries. However, the β-TCP chemistry negatively influenced cell spreading. Besides, another chemical effect was observed as the decrease of the polar component of surface energy on gold-coated samples leaded to a decreased protein adsorption but to an increased seeding efficacy.

References

1. L. HAO and J. LAWRENCE, *Colloid. Surface B* **34** (2004) 87
2. S. B. KENNEDY, N. R. WASHBURN, C. G. SIMON and E. J. AMIS, *Biomaterials* **27** (2006) 3817
3. K. L. KILPADI, P. L. CHANG and S. L. BELLIS, *J. Biomed. Mater. Res.* **57** (2001) 258
4. C. YONGLI, Z. XIUFANG, G. YANDAO, Z. NANMING, Z. TINGYING and S. XINQI, *J. Colloid Interf. Sci.* **214** (1999) 38
5. R. G. LEBARON and K. A. ATHANASIOU, *Tissue Eng.* **6** (2000) 85
6. A. A. SAWYER, K. M. HENESSY and S. L. BELLIS, *Biomaterials* **26** (2005) 1467
7. D. T. HUGHES WASSELL, R. C. HALL and G. EMBERY, *Biomaterials* **16** (1995) 697
8. Q. LUO and J. D. ANDRADE, *J. Colloid Interf. Sci.* **200** (1998) 104
9. K. CAI, J. BOSSERT and K. D. JANDT, *Colloid. Surface B* **49** (2006) 136
10. B. WOJCIAK-STOTHARD, A. CURTIS, W. MONAGHAN, K. MACDONALD and C. WILKINSON, *Exp. Cell. Res.* **223** (1996) 426
11. Y. F. DUFRÊNE, T. G. MARCHAL and P. G. ROUXHET, *Langmuir* **15** (1999) 2871
12. S. G. PENN, L. HE and M. J. NATAN, *Curr. Opin. Cell Biol.* **7** (2003) 609
13. S. V. DOROZHKIN and M. EPPLE, *Angew. Chem. Int. Ed. Engl.* **41** (2002) 3130
14. A. L. OLIVEIRA, P. B. MALAFAYA and R. L. REIS, *Biomaterials* **24** (2003) 2575
15. K. BENZARTI, C. PERRUCHOT and M. M. CHEHIMI, *Colloid. Surface A* **286** (2006) 78
16. D. K. OWENS and R. C. WENDT, *J. Appl. Polym. Sci.* **13** (1969) 1741
17. M. J. DALBY, *Med. Eng. Phys.* **27** (2005) 730
18. L. PONSONNET, V. COMTE, A. OTHMANE, C. LAGNEAU, M. CHARBONNIER, M. LISSAC and N. JAFFREZIC, *Mat. Sci. Eng. C* **21** (2002) 157
19. J. Y. WONG, J. B. LEACH and X. Q. BROWN, *Surf. Sci.* **570** (2004) 119
20. S. RAYNAUD, E. CHAMPION and D. BERNACHE-ASSOLANT, *Biomaterials* **23** (2002) 1073
21. H. S. RYU, H. J. YOUN, K. S. HONG, B. S. CHANG, C. K. LEE and S. S. CHUNG, *Biomaterials* **23** (2002) 909
22. P. MIRANDA, E. SAIZ, K. GRYN and A. P. TOMSIA, *Acta Biomater.* **2** (2006) 457
23. S. BAILLIEZ and A. NZIHOU, *Chem. Eng. J.* **98** (2004) 141
24. J. LONG, M. N. HYDER, R. Y. HUANG and P. CHEN, *Adv. Colloid Interf. Sci.* **118** (2005) 173
25. M. HAN, A. SETHURAMAN, R. S. KANE and G. BELFORT, *Langmuir* **19** (2003) 9868
26. F. L. YAP and Y. ZHANG, *Biosens. Bioelectron.* **22** (2007) 775
27. A. DABROWSKI, *Adv. Colloid Interf. Sci.* **93** (2001) 135
28. N. J. HALLAB, K. J. BUNDY, K. O'CONNOR, R. L. MOSES and J. J. JACOBS, *Tissue Eng.* **7** (2001) 55
29. T. G. Van KOOTEN, H. T. SPIJKER and H. J. BUSSCHER, *Biomaterials* **25** (2004) 1735
30. B. G. KESELOWSKY, D. M. COLLARD and A. J. GARCIA, *J. Biomed. Mater. Res.* **66A** (2002) 247
31. G. K. TOWORFE, R. J. COMPOSTO, C. S. ADAMS, I. M. SHAPIRO and P. DUCHEYNE, *J. Biomed. Mater. Res.* **71** (2004) 449
32. K. WEBB, V. HLADY and P. A. TRESCO, *J. Biomed. Mater. Res.* **41** (1998) 422
33. S. J. LEE, G. KHANG, Y. M. LEE and H. B. LEE, *J. Colloid Interf. Sci.* **259** (2003) 228

34. J. H. LEE, S. J. LEE, G. KHANG and H. B. LEE, *J. Colloid Interf. Sci.* **230** (2000) 84

35. L. MHAMDI, C. PICART, C. LAGNEAU, A. OTHMANE, B. GROGOGEAT, N. JAFFREZIC, L. PONSONNET, *Mat. Sci. Eng. C* **26** (2006) 273

36. X. LIU, J. Y. LIM, H. J. DONAHUE, R. DHURJATI, A. M. MASTRO and E. A. VOGLER, *Biomaterials* **28** (2007) 4535

37. H. M. KOWALCZYNSKA, M. NOWAK-WYRZYKOWSKA, R. KOLOS, J. DOBKOWSKI and J. KAMINSKY, *J. Biomed. Mater. Res.* **72** (2005) 228

38. H. M. KOWALCZYNSKA and M. NOWAK-WYRZYKOWSKA, *Cell Biol. Int.* **27** (2003) 101

39. S. A. REDEY, M. NARDIN, D. BERNACHE-ASSOLANT, C. REY, P. DELANNOY, L. SEDEL and P. J. MARIE, *J. Biomed. Mater. Res.* **50** (2000) 353

40. G. ALTANKOV and T. GROTH, *J. Mater. Sci. Mater. Med.* **5** (1994) 732

41. L. PONSONNET, K. REYBIER, N. JAFFREZIC, V. COMTE, C. LAGNEAU, M. LISSAC and C. MARTELET, *Mat. Sci. Eng. C* **23** (2003) 551

42. A. S. SANTIAGO, E. A. DOS SANTOS, M. S. SADER, M. S. SANTIAGO and G. A. SOARES, *Braz. Oral. Res.* **19** (2005) 203

43. R. QUIRK, W. C. CHAN, M. C. DAVIES, S. J. B. TENDLER and K. M. SHAKESHEFF, *Biomaterials* **22** (2001) 865